Exp. Eye Res. (2002) **74**, 473–482
doi:10.1006/exer.2001.1157, available online at http://www.idealibrary.com on IDEAL®

Cellular Incursion into Bowman's Membrane in the Peripheral Cone of the Keratoconic Cornea

T. SHERWIN[a*], N. H. BROOKES[a], I.-P. LOH[a], C. A. POOLE[b] AND G. M. CLOVER[a]

[a]*Discipline of Ophthalmology, Faculty of Medicine and Health Sciences, University of Auckland, Auckland, New Zealand and* [b]*Division of Anatomy with Radiology, Faculty of Medicine and Health Sciences, University of Auckland, Auckland, New Zealand*

(*Received Seattle 26 July 2001 and accepted in revised form 21 November 2001*)

Analysis of corneal tissue from normal and keratoconic donors has revealed differences which may represent early signs in the pathogenesis of keratoconus. Peripheral areas of keratoconic tissue obtained from transplant surgery were targeted to ascertain cellular disposition and morphological changes which may be masked within the extensive damage of the central keratoconic cone. Peripheral keratoconic corneae exhibited discrete incursion of fine cellular processes into Bowman's membrane. These processes originated from keratocytes and were often observed in conjunction with a defined indentation from the basal epithelium. Comparison of the lysosomal enzymes cathepsin B and G with constitutively expressed cytoplasmic esterase determined that both cathepsins were elevated within keratocytes of keratoconic tissue compared with normal tissue. Some clusters of keratoconic keratocytes had elevated levels of cathepsin exceeding all others. Cathepsin-rich keratocytes localized with morphologically compromised regions of Bowman's membrane. The presence of cell nests deeper within the stroma indicated that the catabolic changes, which are visible within the acellular Bowman's membrane, are probably also occurring deeper within the stroma, but are masked and not readily detectable.

Key words: cornea; keratoconus; keratocyte; epithelium; Bowman's membrane; cathepsin B; cathepsin G.

1. Introduction

Corneal Structure

The stroma of normal corneae is a highly ordered complex structure comprising interspersed lamellae of cells and collagen. Each lamella is 2–3 μm thick and the number of lamellae is uniform. The nature of the keratocyte layers has been re-evaluated in the laboratory using fixable cytoplasmic dyes which enabled identification of three morphologically distinct cell populations in the anterior, central and posterior stroma (Poole et al., 1996). Ramping cell body and cell process connections between adjacent cell layers were also visualized. Evidence for the functionality of anatomically identified cell contacts was provided by the imaging of immunohistochemically labelled gap junction proteins (connexins) in stromal keratocytes (Clover et al., 1996a, Clover et al., 1996b). The distribution of gap junction proteins within the normal corneal epithelium has also been shown previously (Dong et al., 1994).

The disease state of keratoconus is characterized by progressive thinning of the cornea (for review see Rabinowitz, 1998). Transmission electron microscopy (TEM) studies of diseased tissue have revealed that the thickness of collagen lamellae in keratoconus is unaltered, but the number of lamellae appears to be significantly less in normal tissue (Takahashi et al., 1990). Synchrotron X-ray diffraction studies indicate that there is no difference in interfibrillar collagen spacing, hence thinning of the cornea is not due to closer packing of the collagen fibrils within the stroma (Fullwood et al., 1992). This suggests progressive loss of lamellae from the stroma, but how this loss is initiated and the fate of the collagen and keratocytes are unknown. However, low angle X-ray scattering has shown that the orientation of collagen fibrils within the lamellae is altered in keratoconus (Daxer and Fratzl, 1997), suggesting that loss of structural integrity, degradation and/or insufficient repair mechanisms may all be important in the disease process. Cellular involvement in these degradative processes remains unclear, although differences in keratocyte morphology and cell–matrix interactions have been shown by high voltage electron microscopy (Rock et al., 1995).

Extracellular Matrix Proteins

The literature describing collagen levels in keratoconic corneae is inconclusive: Critchfield et al. (1988) described decreased collagen and total protein levels

* Address correspondence to: Trevor Sherwin, Discipline of Ophthalmology, Faculty of Medicine and Health Sciences, Private Bag 92019, University of Auckland, Auckland, New Zealand. E-mail: t.sherwin@auckland.ac.nz

0014-4835/02/$35.00/0

in keratoconic tissue by western blotting. Radda et al. (1982) found a 5 % increase in type I collagen in keratoconus, while Zimmermann et al. (1988) found no differences in collagen composition of biochemical extracts from keratoconus. Analysis of expression of collagens by keratocytes in cell culture further clouds the issue: Newsome et al. (1981) stated that collagen types I and III were synthesized in similar amounts by both normal and keratoconic derived stromal cells, while Peters et al., (1993) analysed four cultures of keratoconic cells and found that type I collagen and steady-state RNAs were reduced in cells from three of the four cultures. The answer to these apparent anomalies may lie in the work of Yue et al., (1985). These authors analysed the translational activity of total RNA from cells derived from keratoconic corneae and found two distinct groups. One group of keratoconic cells showed the same amount of total RNA and the same rate of mRNA synthesis as normal cells, whilst the other keratoconic group contained more total RNA than normal cells, but the translational efficiency was so low that there was a marked reduction in protein synthesis. This suggests that the situation in the keratoconic stroma is complex and that groups of cells may be acting differently to each other. This is intriguing considering the high degree of interconnectivity and profusion of gap junctions known to exist in normal stroma (Clover et al., 1996a,b).

Type VI collagen is a major component of the extracellular matrix in human cornea (Zimmerman et al., 1986; Reale et al., 2001) and is thought to be involved in mediating matrix–matrix and cell–matrix interactions. Cultures of keratoconic stromal cells produce no detectable levels of type VI collagen, whilst in control cultures it is easily detectable (Chwa et al., 1996). Such interruption of type VI collagen production would undoubtedly affect the matrix–matrix and cell–matrix interactions of the cornea and could lead to the structural aberrations observed in the advanced state of keratoconic disease.

Proteolytic Enzymes

Altered levels of proteolytic enzymes and their inhibitors have been reported in keratoconic corneae. Rehany et al. (1982) first showed increased collagenolytic activity in keratoconic compared to normal corneae, while Kenney et al. (1989) found altered gelatinase (MMP 2) activity in similar groups. Sawaguchi et al. (1990) noted a 75 % reduction in α1 proteinase inhibitor, while Fukuchi et al. (1994) showed increased levels of lysosomal hydrolases in the conjunctival epithelia of deceased keratoconic patients. More recently, in situ hybridization studies have reported increased mRNA levels for cathepsin G and decreased mRNA levels for α1 proteinase inhibitor (Whitelock et al., 1997). Confirmation at the protein level was provided by Zhou et al. (1998), who found increased levels of cathepsins B and G in keratoconic corneae by immunofluorescence and Western blotting, while no changes were found in the levels of several catabolic matrix metalloproteinases (MMPs 1, 2, 3 and 9). Despite these contradictory findings, it is interesting that the studies of Kielty et al. (1993) described the degradation of microfibrillar type VI collagen by cathepsin G, but not by MMPs like stromelysin (MMP 3), collagenase (MMP 1) and gelatinase (MMP 2) which are typically involved in the extracellular turnover of types I and III collagen.

Bowman's Membrane

Structural abnormalities and defects in Bowman's membrane in the central part of keratoconic cornea have been well documented. Sawaguchi et al. (1998) examined the collagen network in keratoconic tissue by scanning electron microscopy and found sharply edged defects and ruptures in Bowman's layer to varying degrees in all corneae examined. Tuori et al. (1997) noted discontinuities in Bowman's layer and sometimes distorted stroma beneath these defects. Kenney et al. (1997) noted gaps in Bowman's and also observed fibrotic regions where the epithelium was in direct contact with the stroma. These authors also observed that abnormalities of the extracellular matrix were not uniform within an individual keratoconic cornea again suggesting localized areas of disease progression.

Most studies of keratoconus tend to target the central cone of the corneae for analysis, since this is the area of greatest disease involvement. However, the major structural changes associated with corneal thinning and cone formation may mask many of the underlying mechanisms driving this disease process. In this study, the authors targeted the peripheral cone area of keratoconic corneae to determine if cellular changes in this region could be used to identify early pathological events which would otherwise be masked by the major structural damage that occurs in the central cone of the keratoconic corneae.

2. Materials and Methods

Tissue Origin

This study used normal human corneal tissue donated for research via the New Zealand National Eye Bank (six samples) and keratoconic corneal tissue (10 samples) obtained from recipients of corneal grafts via Auckland Public Hospital. Grafting criteria require visual acuity of 6/24 or worse.

Light Microscopy

Corneal segments were labelled with 5-chloromethylfluorescein diacetate (CMFDA) (Molecular Probes Inc., U.S.A.) as previously described (Poole

et al., 1996) and fixed in freshly prepared 2% paraformaldehyde for 10–20 min. Following washing with media the sample was processed for cryosectioning.

Cryosectioning

Corneal segments were mounted in an antero-posterior orientation and frozen in OCT. Sections of 30 μm through the complete depth of the tissue were dried onto numbered, poly-L-lysine coated slides.

Immunohistochemistry

Immunohistochemical techniques were adapted to suit the requirements of both epitopes and antibodies. Labelling of intracellular epitopes required permeabilization of the cell membranes (−20°C methanol, 5 min). Triple labelling of tissue was performed using discrete emission wavelength fluorophores to reveal each protein structure (Clover et al., 1996b).

Antibodies

Details of antibodies and fluorophores are presented in Table I.

Confocal Microscopy

Optical sectioning of labelled tissue was examined using a Leica TCS 4d Confocal Laser Scanning microscope based on a Leica DMRB microscope. This microscope is fitted with a krypton–argon mixed gas laser with four excitation lines. Sections of tissue were observed using high numerical aperture oil immersion lenses at varying magnifications (40×, 63× and 100×). Z-series data sets were collected at approximately 1 μm intervals.

Image Processing

Confocal images were processed in two ways:

1. Z-series images were processed with Leica scanware into an extended focus image, where all the 3D information is combined into a single 2D image with all the data in focus at once.
2. Z-series images were volume rendered using VoxelView on a Silicon Graphics Iris Indigo workstation. Volumes were then digitally sectioned in three orientations in each channel before importing into 'MicroIMAGEBASE' software created in the laboratory using iShell (Tribeworks Inc.) (Brookes et al., 2001).

Image Quantitation

Digital confocal images were imported into NIH Image and fluorescence intensities were topographically mapped. Analysis of the enzyme levels within individual keratocytes in the anterior stroma of keratoconic corneas was performed using 3D height maps which translate the fluorescence intensity levels (0–255) from digital images of corneal tissue into topographical maps. Images were then density sliced to exclude low level background fluorescence and individual cells were analysed with respect to mean fluorescence intensity in each of the fluorophore channels. To eliminate variations in cathepsin labelling caused by variations in cell volume and/or cell bodies partially within the section, cathepsin labelling intensities were normalized against the corresponding intensity of a constitutively expressed enzyme within the same cell, namely, esterase which is the target recognized by CMFDA labelling. Enzyme intensities were then expressed as a ratio of cathepsin/esterase and final data were then imported into Microsoft Excel for statistical analysis.

TABLE I

Details of antibodies and fluorophores

Antibody	Description	Dilution	Source
Cathepsin B	Sheep anti-human	1:250	Serotec, AHP18H
Cathepsin G	Sheep anti-human	1:50	ICN Biomedicals, 64-732
Vimentin	Mouse monoclonal	1:100	Sigma, V6630
α3β1 P1B5 integrin	Mouse monoclonal anti-human	1:100	DAKO, M608
Alexa 546	Goat anti-mouse IgG secondary antibody	1:1000	Molecular Probes, A11003
Biotinylated donkey anti-sheep IgG	Biotin-conjugated secondary antibody	1:1000	Sigma, B-7390
Biotinylated goat anti-mouse IgG	Biotin-conjugated secondary antibody	1:1000	Sigma, B-7264
Streptavidin-linked Cy5	Tertiary molecule	1:200	Amersham, PA45001

3. Results

Ten keratoconic corneae removed during keratoplastic surgery and six normal corneae obtained during post-mortem were processed for examination by confocal microscopy, ex vivo and in situ. Immunohistochemistry using specific probes revealed abnormal cellular features apparent within the keratoconic corneal buttons, but absent within normal controls. The cellular architectural changes observed in keratoconic tissue indicated interactions between epithelium and keratocytes.

Cellular Appearance of the Central Keratoconic Cone

Observation of antero-posterior sections through keratoconic corneae showed thinning and structural deterioration of the cornea, reducing the corneal thickness to 378 μm in the central cone area as shown using CMFDA to define cellular detail in Fig. 1.

Cellular features that concur with previous structural studies (Kenney et al., 1997; Tuori et al., 1997; Sawaguchi et al., 1998) are clearly visible. The central cornea is disrupted with loss of organization of cellular and collagen lamellae. The normally acellular Bowman's membrane shows thinning centrally, supported by the continuity of CMFDA labelling between epithelium and stroma. Of interest is the severely thickened epithelial layer which is 12 cells deep in parts, a thickness of approximately 108 μm. Combining this data with the overall thickness of the cornea at the central cone previously mentioned means that the effective stromal thickness in this area is less than 270 μm.

Cellular Incursion at the Peripheral Keratoconic Cone

Examination of areas peripheral to the central keratoconic cone revealed much more localized disruptions of Bowman's membrane than were observed within the central cone. Discrete cell processes were observed within Bowman's membrane which completely traversed the normally acellular layer to link the stroma with the epithelium (Fig. 2(A)). In this example, extremely fine cellular elements were noted adjacent to the cell process (Fig. 2(A)). Using a probe to the intermediate filament protein vimentin, the cell processes crossing Bowman's membrane were determined to be of mesenchymal origin (Fig. 2(B)) and therefore to be keratocytic in nature. The extremely fine cellular material in close proximity to these processes also stained positively for vimentin and therefore originated from cellular elements within the stroma.

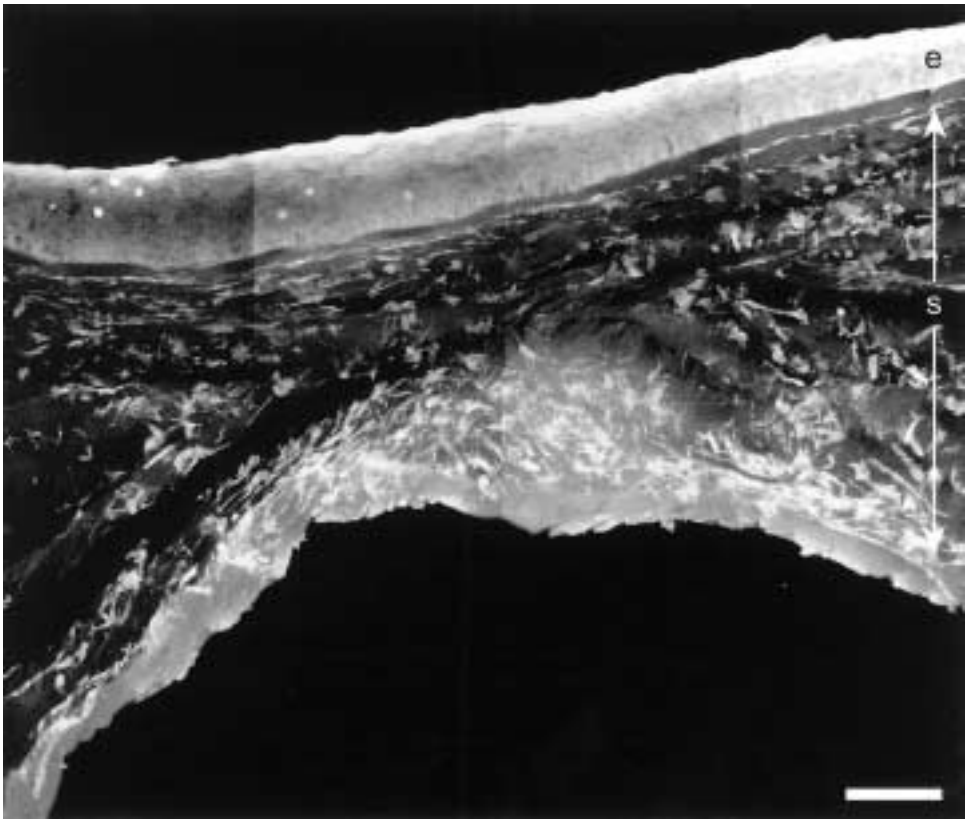

FIG. 1. Cellular architecture revealed in the central 1000 μm of the keratoconic tissue using CMFDA labelling (bar = 100 μm). Antero-posterior sections of tissue were imaged at high magnification and multiple adjacent images were reconstructed into a composite image to reveal the features of the keratoconic cone at high resolution. Features include severe thinning of the corneal stroma (s), thickening of the epithelium (e) and disruption of the normal cellular architecture of the stroma.

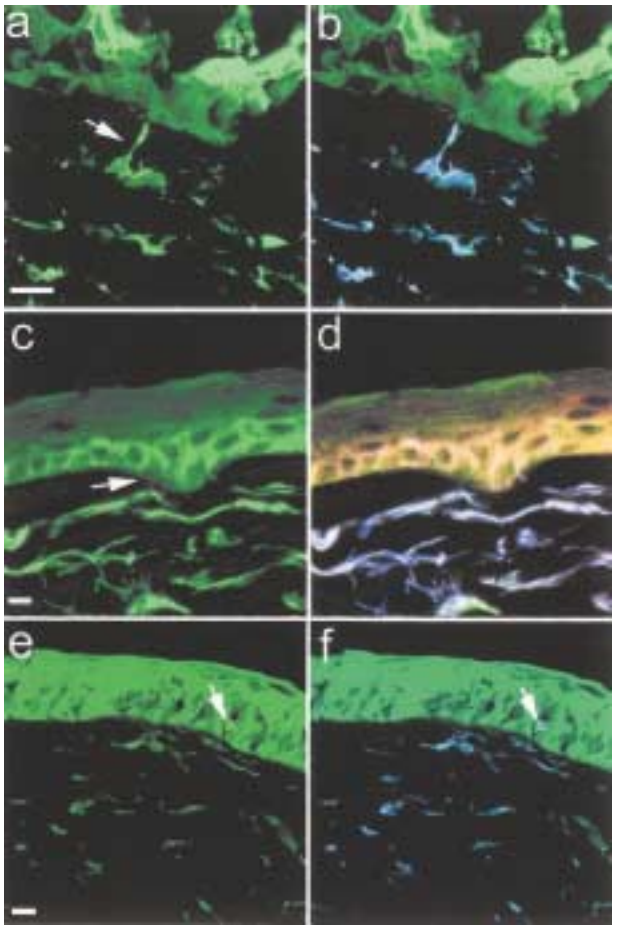

FIG. 2. A Peripheral area of keratoconic tissue displaying cellular material within Bowman's membrane (A, bar = 10 μm). One major cell process (arrow) and several adjacent fine processes are observed. lmmunolabelling with vimentin (blue, B) reveals the keratocyte origin of these processes. Areas of keratocyte incursion are often accompanied by epithelial invagination seen using CMFDA labelling (arrow, C, bar = 10 μm). Confirmation of cellular origin is defined in (D) using vimentin to highlight keratocytes (blue) and integrin α3β1 to highlight basal epithelium (red). Keratocyte invasion of the epithelium was observed in two tissue samples. One example is depicted in (E) and (F) where anomalies within the basal epithelium (arrow, E, bar = 20 μm) are confirmed to be keratocytes using vimentin labelling (arrow, F). The fluorophores used to reveal vimentin and integrin labelling were Alexa 546 and Cy5, respectively.

Epithelial Invagination of Bowman's Membrane

The appearance of cellular material within the acellular Bowman's membrane was also observed to be coincident with invaginations of the epithelium (Fig. 2(C)). Groups of epithelial cells dipped down into Bowman's membrane with a bell-shaped appearance and were coincident with keratocyte incursion within Bowman's membrane.

Dual immunolabelling with probes to vimentin and the integrin α3β1, normally associated with the basal epithelial layer, elucidated the pathology of these cellular incursions in keratoconic corneae (Fig. 2(D)). The emergence of vimentin positive keratocyte processes within Bowman's membrane was associated with an invagination of epithelial cells which stain positively for integrin α3β1. At the point of invagination, the staining with α3β1 appeared to be two cells deep in comparison with the normal staining of just the most basal cell layer. These stromal and epithelial abnormalities were observed in the peripheral cone of all 10 keratoconic corneas examined.

In two keratoconic corneae, extreme cases of cellular interaction were observed. In the example illustrated, disruption of basal epithelial cells (Fig. 2(E)) correlated with the invasion of vimentin positive keratocytes migrating in from the stroma (Fig. 2(F)).

Three-dimensional Investigation of Cell Processes within Bowman's Membrane

Confocal microscopy followed by three-dimensional reconstruction has elucidated the interaction of cells within Bowman's membrane in keratoconus.

Using microlMAGEBASE software developed within the laboratory, it is possible to view volumes of corneal tissue in three dimensions in real time. Still images captured from within microlMAGEBASE are shown in Fig. 3 to illustrate the 3D nature of the cell processes within Bowman's membrane.

Fig. 3(A) shows the extended focus view of an antero-posterior section of a keratoconic cornea displaying the features of keratocyte processes within Bowman's membrane and inward invagination of the opposing epithelium. CMFDA identifies living cells while α3β1 integrin is labelled red and denotes the basal epithelium. Because Fig. 3(A) is an extended focus image, it actually represents a three-dimensional volume of tissue when viewed from the top (*z*-axis). Thus, using the microlMAGEBASE software, information from particular optical sections in the other two planes (*X* and *Y*-axes) can be extracted from the volume by viewing from the bottom and right, respectively.

Fig. 3(B) shows an optical slice looking in from the right-hand side of the volume at the position marked in Fig. 3(A). The cell projection within Bowman's layer appears to flatten as it contacts the epithelium. This cell projection is also clear when viewed from the third axis, looking in from the bottom of the volume at the position marked in Fig. 3(E).

Analysis of Figs 3(A), (B) and (E) clearly defines the cellular material within Bowman's membrane as a discrete cell projection emanating from a keratocyte within the stroma.

Three-dimensional Analysis of Epithelial Indentations in Bowman's Membrane

A series of three optical slices through the epithelial indentation in Fig. 3(A) (at the points marked) viewed from the bottom of the volume are shown in Figs 3(E),

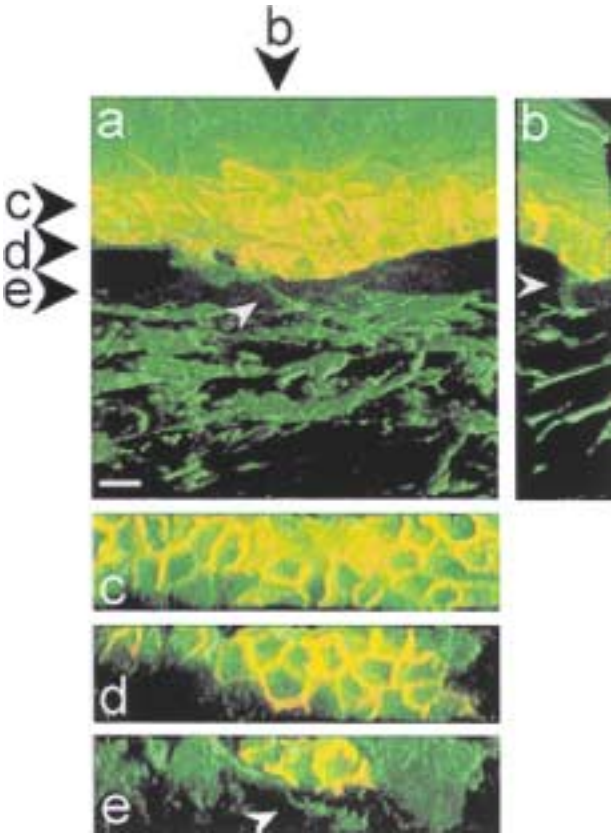

FIG. 3. Three-dimensional analysis of areas of compromised Bowman's membrane in keratoconic tissue reveals the morphology of keratocytic and epithelial incursion. An extended focus image of an antero-posterior volume of tissue labelled with CMFDA, to reveal vital cells (green) and α3β1 integrin to reveal basal epithelium (red), is shown in (A), (bar = 10 μm). Co-localization of red and green pixels results in a yellow hue. The view of this tissue volume looking into it from the top (A), right (B) and from the bottom (E) at the position shown by the arrows on the top view determines the keratocyte cellular process as a discrete entity in three dimensions (arrowheads). Furthermore, sequential views of the tissue volume (E, D and C) viewed from the bottom of the extended focus (A) at the positions marked show that the labelling of basal epithelium, as seen by α3β1 integrin labelling, progresses to a discrete dimple-shaped invagination.

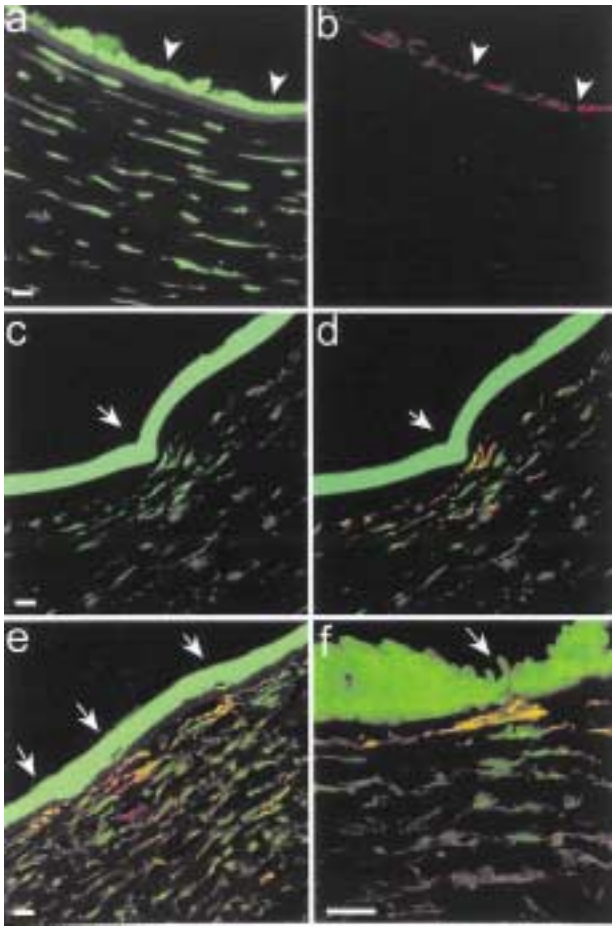

FIG. 4. Sections of corneal tissue labelled with CMFDA (green) and cathepsin B (red, Alexa 546) are depicted in (A)–(F). Normal corneal tissue exhibits little cathepsin B labelling within the stroma (B) compared to esterase labelling (A, bar = 20 μm), the position of the epithelium is marked by arrowheads. Keratoconic tissue shows increased cathepsin B labelling (D, red) when overlaid on the esterase-labelled image (D, green). CMFDA labelling alone is shown in (C) (bar = 20 μm). Epithelial and stromal compromisation of Bowman's membrane are marked (arrow). Further examples of cathepsin B distribution (red, E and F) in keratoconic tissue are seen overlaid on the CMFDA image (green). Co-localization of red and green pixels results in a yellow hue. Areas of compromisation of Bowman's membrane are arrowed.

(D) and (C). The even distribution of α3β1 integrin in Fig. 3(C) indicates that the basal epithelium is level within this optical section. However, as the optical slices progress towards Bowman's membrane (Fig. 3(D)), the integrin-staining pattern becomes localized to the central portion with no staining at the periphery. Ultimately, the integrin distribution comes to a finite apex in Fig. 3(E), being distributed around only three basal epithelial cells. It is at this point that the keratocyte process which extends through Bowman's membrane contacts the epithelium.

Cathepsin Distribution Within the Anterior Keratoconic Cornea

Normal corneal sections immunohistochemically labelled for cathepsins B and G exhibited extremely weak staining patterns. The highest levels of both enzymes were present within the epithelium, while the enzyme was barely visible in stromal keratocytes (Fig. 4(B)). Dual labelling for cathepsin B and G revealed identical staining patterns for both enzymes, but only cathepsin B images were used for illustration to avoid duplication. Comparison with the endogenous esterase level (Fig. 4(A)) accentuates the low cathepsin B levels (Fig. 4(B)), particularly since merging the two images renders the cathepsin labelling invisible.

Tissue samples from the three most recently acquired keratoconic corneas processed and dual labelled with CMFDA and antibodies to cathepsin B revealed distinctly different enzyme ratios compared to normal cornea. Areas peripheral to the central keratoconic cone were examined for the predictive morphology of

keratocyte cell processes within Bowman's membrane and/or epithelial indentation as indicated by CMFDA labelling. These areas were subsequently examined for cathepsin distribution.

Fig. 4(C) shows a peripheral area displaying the cellular morphology of keratocyte material within Bowman's membrane and concurrent indentation of the epithelium as seen by CMFDA labelling. The cathepsin B distribution in this area overlayed in the red channel (Fig. 4(D)) shows significantly higher levels of the enzyme in keratocytes than was observed in normal corneal samples. Significantly, the most intense staining was found in keratocytes associated with the compromised site in Bowman's membrane. However, not all of the keratocytes within the group adjacent to epithelial indentation show elevated levels of cathepsin enzyme. The second example depicted in Fig. 4(E) displays an area of anterior keratoconic cornea which contains three discrete sites of compromised Bowman's membrane. The cathepsin concentration within the keratocytes (red) is elevated at each of the three sites and yet the keratocytes between the sites exhibit much lower levels of cathepsin. Higher magnification (Fig. 4(F)) confirms that the cathepsin levels are elevated within the cells which are in contact with the epithelium compared with the basal levels within the adjacent keratocytes.

Quantitation of Cathepsin Levels Within Individual Keratocytes

Analysis of the enzyme levels within individual keratocytes was performed using fluorescence intensity topographical maps. Fig. 5(B) shows the intensity topographical map for cathepsin B within the image previously shown in Fig. 4(E). The cells with the most intense staining for cathepsin are apparent as the highest peaks within the intensity map. This can be compared with the topographical map for CMFDA (Fig. 5(A)) which shows much higher intensity levels overall and is more evenly distributed within the keratocytes of the stroma.

The mean fluorescence intensity of cathepsin labelling was determined for 68 individual keratocytes in this tissue section. The results are displayed as intensity levels for each cell in Fig. 6(A). The corresponding intensity levels of a constitutively expressed enzyme, namely esterase, which is the target recognized by CMFDA labelling was also determined and the corresponding trace for each cell is also depicted in Fig. 6(A).

Enzyme intensities were then expressed as a ratio of cathepsin/esterase and ordered according to relative intensity shown in Fig. 6(B). Analysis of this graph reveals that there is a straight line increase in cathepsin/esterase ratio illustrating a statistically normal variation in distribution, until the latter points assume a dramatic increase in enzyme distribution (Fig. 6(B), arrow). These final six points on the graph, representing six cells out of the 68 analysed showed a

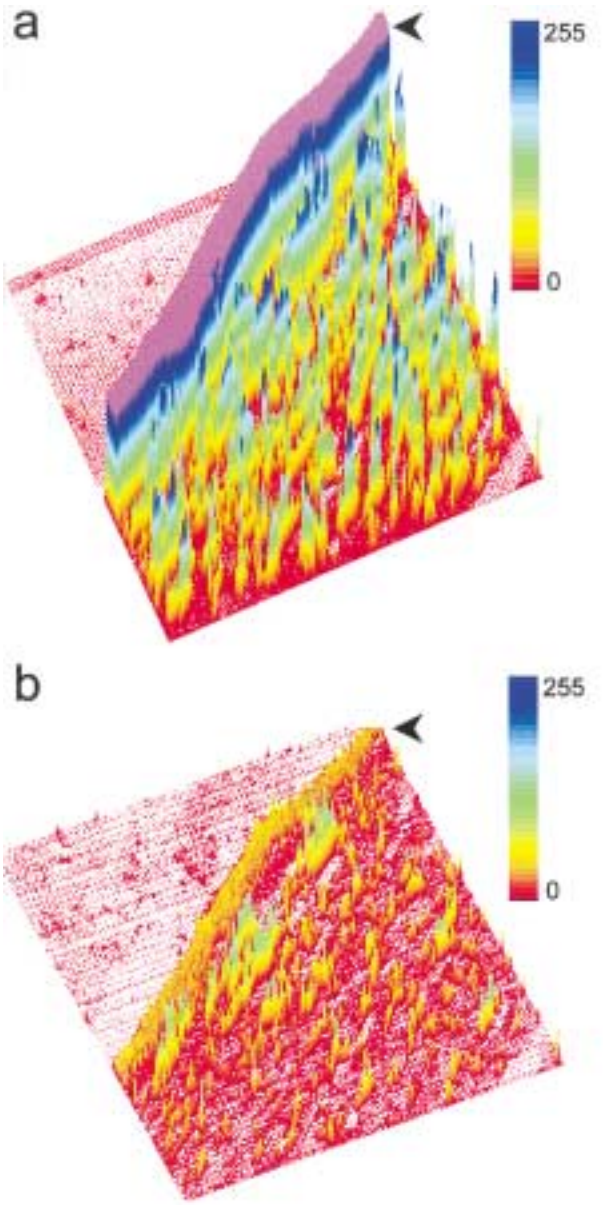

FIG. 5. Topographical maps of enzyme intensity within the tissue sample previously shown in Fig. 4(E) demonstrate the localized distribution of cathepsin B labelling. Cathepsin B labelling fluorescence intensity (B, represented on a scale of 0–255) shows much more localized foci than the constitutive esterase labelling (A) although the esterase labelling exhibits generally much higher intensities. Epithelium is indicated with arrowheads.

significant increase in the cathepsin/esterase ratio. The cells constituting the latter phase of the graph displayed a mean intensity ratio of $0{\cdot}57 \pm 0{\cdot}09$ compared to a mean intensity ratio of $0{\cdot}34 \pm 0{\cdot}06$ within the cells prior to the nexus ($P < 0{\cdot}0025$). Identification of the keratocytes expressing significantly higher levels of cathepsin, compared to constitutive esterase, by pseudocolouring red on the original image, revealed that three cathepsin positive keratocytes coincided with breaks in Bowman's membrane (Fig. 6(C)) and three others occurred several cell layers back within the corneal stroma.

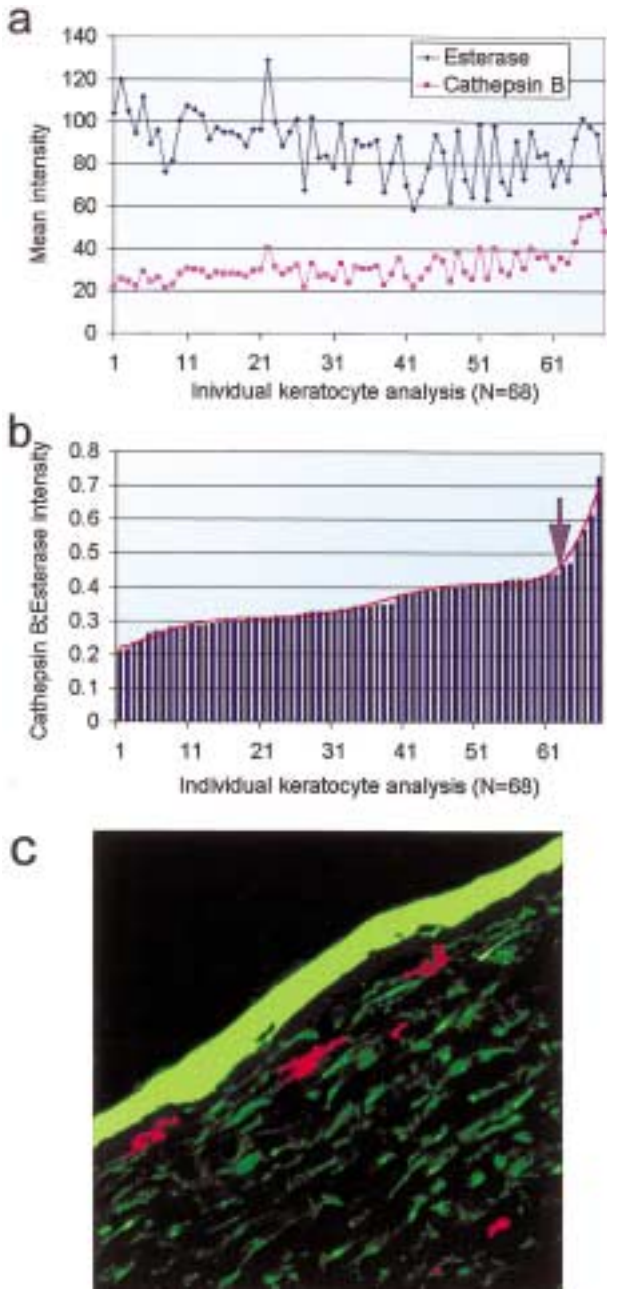

FIG. 6. Mean intensities of esterase and cathepsin B labelling analysed per cell (68 cells analysed) for the keratoconic sample from Fig. 4(E) show expected fluctuating variations (A). However, expression of the data as a ratio of cathepsin B fluorescence intensity/esterase fluorescence intensity and ordering of the cells according to increasing ratio (B) reveals a significant increase in cathepsin B intensity in a small proportion of the cells. The nexus in cathepsin B labelling intensity is arrowed. The cells lying above the nexus in (B) have been pseudocoloured in red (C) to show the position of the cathepsin B-rich cells within the tissue sample analysed.

Examination of two other keratoconic samples revealed almost identical results (second keratoconic cornea sample had a mean of $0{\cdot}34 \pm 0{\cdot}055$ prior to the nexus and $0{\cdot}47 \pm 0{\cdot}037$ beyond the nexus, $P < 0{\cdot}001$, while the third keratoconic cornea produced values of $0{\cdot}366 \pm 0{\cdot}078$ prior to the nexus and $0{\cdot}593 \pm 0{\cdot}056$ beyond the nexus, $P < 0{\cdot}001$). Furthermore, the cells that possessed cathepsin levels above the nexus, again were located adjacent to the defects in Bowman's membrane with a proportion of cathepsin-rich cells further back in the stroma.

4. Discussion

This study describes a unique examination of the peripheral keratoconic cone to define more precisely, the aberrant behaviour of keratocytes in the disease process, keratoconus. The aberrant behaviour is more readily seen within Bowman's membrane because it is normally acellular, but may also reflect pathological processes normally masked within the deeper stroma. Furthermore, this study represents the first description of the cellular architecture within keratoconic cornea using the vital dye, CMFDA, which enhanced visibility of the fine cellular architecture throughout diseased corneae.

Cellular Incursion into Bowman's Membrane Peripheral to the Keratoconic Cone

This investigation of areas peripheral to the central cone in keratoconic corneas has highlighted abnormalities which may represent early pathological features of the disease that cannot be discerned within the damage observed in the more often studied central region. The microscopical changes described here would not be observable by slit lamp biomicroscopy. Even higher resolution studies of the three-dimensional arrangement of collagen lamellae by scanning electron microscopy noted changes in the apical region, but observed no differences in the para-apical region compared with normal tissue (Radner et al., 1998). Using the laboratory's previously novel technique of CMFDA dye (Poole et al., 1996) to observe corneal cellular morphology within the cornea, this study has revealed pathological changes in the cells which are not evident by routine histological examination.

This work has demonstrated that abnormal appearance of cellular material within Bowman's membrane is observable peripheral to the central cone area in keratoconic corneas. Although abnormalities and breaks in Bowman's membrane have been widely reported within the central cone area, this is the first report of such discrete abnormalities within the peripheral cone. Furthermore, it shows that cellular material occupies the fractures which have been observed in this normally acellular zone. Further work is being undertaken to determine if these defects are specific to keratoconus.

The morphological appearance of the cellular material within Bowman's membrane has implications for the nature of the defects within this zone. The 3D structural analyses showed the defined nature of the keratocyte processes and indicate that the weaknesses within Bowman's are discrete incursions,

containing cellular material, rather than elongated cracks. This view is further supported by the appearance of the epithelial invaginations which were present in conjunction with the keratocyte processes. The convex morphology of the epithelial descent into the collagenous Bowman's layer indicated that these flaws were dimple-shaped as opposed to a ridge or fissure. These observations indicated that the appearance of keratocyte material within Bowman's membrane can occur without epithelial invagination, but that epithelial invagination is always associated with stromal cell processes. This suggests that keratocyte invasion of Bowman's membrane occurs prior to epithelial indentation. Single processes digesting Bowman's membrane would have the effect of a point weakness within the layer. Such localized weaknesses could enlarge over time through continued collagen degradation and exacerbated by physical stress such as eye rubbing or an intraocular pressure which is too great for the increasingly fragile stroma and Bowman's membrane. These small, localized weaknesses could predispose to larger fractures, leading to the breaks in Bowman's layer which are observed in the central keratoconic cone.

The question remains: Does the cellular material actively invade Bowman's membrane or does it passively collapse into an existing defect? The presence in two samples of keratocytes within the basal epithelium suggests an active migration of keratocytes, as opposed to simply filling a gap that has recently appeared in Bowman's membrane.

Cathepsin Enzyme Levels Within Keratocytes in Peripheral Keratoconic Corneas

Levels of cathepsin enzymes have been previously reported as being elevated in keratoconic corneas (Whitelock et al., 1997; Zhou et al., 1998). These reports have concentrated upon the central cone region of the diseased cornea or analysed the tissue as a whole. Here the authors report the analysis of cathepsin levels within individual keratocytes in the peripheral region of the keratoconic cornea. The data showed that a small proportion of the keratocytes in the anterior stroma had strongly elevated levels of cathepsin enzymes compared to a constitutively expressed esterase enzyme. The cells with the highest cathepsin levels occurred in isolated positions, adjacent to keratocytes with much lower levels of the enzyme and most significantly, adjacent to compromised regions of Bowman's membrane. However, the appearance of cathepsin-rich keratocytes at deeper levels within the stroma is indicative of the fact that the cellular disruption of the extracellular matrix observed in Bowman's membrane may also be occurring deeper within the stroma.

The isolated nature of these keratocytes contrasts markedly with the interconnected nature of the corneal keratocyte network. It will be interesting to determine if the cathepsin-rich keratocytes become disconnected from the network and function independently. High levels of cathepsin have been implicated as one of the possible causes of matrix degradation in keratoconus (Zhou et al., 1998). In particular, the ability of cathepsins to degrade type VI collagen (Kielty et al., 1993) may affect the function of type VI collagen which is to promote cell–matrix and matrix–matrix interactions. Obviously, matrix degradation needs to occur in wound healing and matrix remodelling. However, the extremely localized nature of the cathepsin-rich keratocytes makes it unlikely that they are responding to wound healing signals as these types of response are much more widespread.

It is therefore possible that these individual keratocytes, which become isolated from the network, are acting independently and are compounding progression of the disease. The clusters of cathepsin-rich keratocytes may be a manifestation of an early pathological stage in the keratoconic process. These small, localized pockets of activity could coalesce, with time and stress, to form regional areas of expanding disruption eventually leading to the global disease pathology observed within the central cone.

Acknowledgements

This study was supported by grants from the Auckland Medical Research Foundation and the National Keratoconus Foundation, U.S.A. C.A.P. is a Senior Research Fellow of the Health Research Council of New Zealand.

References

Brookes, N. H., Sherwin, T., Loh, I.-P., Poole, C. A. and Clover, G. M (2001). Three dimensional multi-channel imaging in large volumes of corneal stroma. *Microsc. Anal.*, in press.

Chwa, M., Kenney, M. C., Khin, H. and Brown, D. J. (1996). Altered type VI collagen synthesis by keratoconus keratocytes in vitro. *Biochem. Biophys. Res. Commun.* **224**, 760–4.

Clover, G. M., Brookes, N. H. and Poole, C. A. (1996a). Confocal laser scanning microscopy of human corneal keratocytes with co-localized membrane gap junction proteins. *Invest. Ophthalmol. Vis. Sci.* **37**, S1013.

Clover, G. M., Poole, C. A. and Brookes, N. H. (1996b). Confocal imaging of gap junction protein associated with the keratocytes of the human cornea. *Aust. NZ J. Ophthalmol.* **24**, 10–l2.

Critchfield, J. W., Calandra, A. J., Nesburn, A. B. and Kenney, M. C. R. (1988). Keratoconus. I. Biochemical studies. *Exp. Eye Res.* **46**, 953–64.

Daxer, A. and Fratzl, P. (1997). Collagen fibril orientation in the human corneal stroma and its implication in keratoconus. *Invest. Ophthalmol. Vis. Sci.* **38**, 1289–90.

Dong, Y., Roos, M., Gruijters, T., Donaldson, P., Bullivant, S., Beyer, E. and Kistler, J. (1994). Differential expression of two gap junction proteins in corneal epithelium. *Eur. J. Cell Biol.* **64**, 95–100.

Fukuchi, T., Yue, B. J. Y. T., Sugar, J. and Lam, S. (1994). Lysosomal enzyme activities in conjunctival tissues of

patients with keratoconus. *Arch. Ophthalmol.* **112**, 1368–74.

Fullwood, N. J., Tuft, S. J., Malik, N. S., Meek, K. M., Ridgway, A. E. A. and Harrison, R. J. (1992). Synchrotron X-ray diffraction studies of keratoconus corneal stroma. *Invest. Ophthalmol. Vis. Sci.* **33**, 1734–41.

Kenney, M. C., Chwa, M., Escobar, M. and Brown, D. (1989). Altered gelatinolytic activity by keratoconus corneal cells. *Biochem. Biophys. Res. Commun.* **161**, 353–7.

Kenney, M. C., Nesburn, A. B., Burgeson, R. E., Butkowski, R. J. and Ljubimov, A. V. (1997). Abnormalities of the extracellular matrix in keratoconus corneas. *Cornea* **16**, 345–51.

Kielty, C. M., Lees, M., Shuttleworth, A. and Woolley, D. (1993). Catabolism of intact type VI collagen microfibrils: susceptibility to degradation by serine proteinases. *Biochem. Biophys. Res. Commun.* **191**, 1230–6.

Newsome, D. A., Foidart, J. M., Hassell, J. R., Krachmer, J. H., Rodrigues, M. M. and Katz, S. I. (1981). Detection of specific collagen types in normal and keratoconus corneas. *Invest. Ophthalmol. Vis. Sci.* **20**, 738–50.

Peters, D. P., Harrison, D. A. and Brandt, C. R. (1993). Heterogeneity of type I collagen expression in human corneal keratoconus fibroblasts. *Ophthalmic Res.* **25**, 273–9.

Poole, C. A., Brookes, N. H. and Clover, G. M. (1996). Confocal imaging of the keratocyte network in living porcine corneae using the fixable fluoroprobe 5-chloromethylfluorescein diacetate. *Curr. Eye Res.* **15**, 165–74.

Rabinowitz, Y. S. (1998). Keratoconus. *Surv. Opthalmol.* **42**, 297–319.

Radda, T. M., Menzel, E. J., Freylet, H. and Gnad, H. D. (1982). Collagen types in keratoconus. *Graefes Arch. Clin. Exp. Ophthalmol.* **218**, 262–4.

Radner, W., Zehetmayer, M., Skorpik, C. and Mallinger, R. (1998). Altered organization of collagen in the apex of keratoconus corneas. *Ophthalmic Res.* **30**, 327–32.

Reale, E., Groos, S., Luciano, L., Eckardt, C. and Eckardt, U. (2001). In the mammalian eye type VI collagen tetramers form three morphologically different aggregates. *Matrix Biol.* **20**, 37–51.

Rehany, U., Lahav, M. and Shoshan, S. (1982). Collagenolytic activity in keratoconus. *Ann. Ophthalmol.* **14**, 751–4.

Rock, M. E., Moore, M. N., Anderson, J. A. and Binder, P. S. (1995). 3-D computer models of human keratocytes. *CLAO J.* **21**, 57–60.

Sawaguchi, S., Fukuchi, T., Abe, H., Kaiya, T., Sugar, J. and Yue, B. T. Y. T. (1998). Three dimensional scanning electron microscopic study of keratoconus corneas. *Arch. Ophthalmol.* **116**, 62–8.

Sawaguchi, S., Twining, S. S., Yue, B. Y., Wilson, P. M., Sugar, J. and Chan, S. K. (1990). Alpha-1 proteinase inhibitor levels in keratoconus. *Exp. Eye Res.* **50**, 549–54.

Takahashi, A., Nakayasu, K., Okisaka, S. and Kanai, A. (1990). Quantitative analysis of collagen fibres in Keratoconus. *Acta Soc. Ophthalmol. Jpn.* **90**, 1068–73.

Tuori, A. J., Virtanen, I., Aine, E., Kalluri, R., Miner, J. H. and Uusitalo, H. M. (1997). The immunohistochemical composition of corneal basement membrane in keratoconus. *Curr. Eye Res.* **16**, 792–801.

Woods, A., Sherwin, T., Sasse, R., MacRae, T. H., Baines, A. J. and Gull, K. (1989). Definition of individual components within the cytoskeleton of *Trypanosoma brucei* by a library of monoclonal antibodies. *J. Cell Sci.* **93**, 491–500.

Whitelock, R. B., Fukuchi, T., Zhou, L., Twining, S. S., Sugar, J., Feder, R. S. and Yue, B. Y. J. T. (1997). Cathepsin G, acid phosphatase and alpha-1-proteinase inhibitor messenger RNA levels in keratoconus corneas. *Invest. Ophthalmol. Vis. Sci.* **38**, 529–34.

Yue, B. Y. J. T., Sugar, J. and Beneviste, K. (1985). RNA metabolism in cultures of corneal stromal cells from patients with keratoconus. *Proc. Soc. Exp. Biol. Med.* **178**, 126–32.

Zhou, L., Sawaguchi, S., Twining, S. S., Sugar, J., Feder, R. S. and Yue, B. Y. (1998). Expression of degradative enzymes and protease inhibitors in corneas with keratoconus. *Invest. Ophthalmol. Vis. Sci.* **39**, 1117–24.

Zimmermann, D. R., Fischer, R. W., Winterhalter, K. H., Witmer, R. and Vaughan, L. (1988). Comparative studies of collagens in normal and keratoconus corneas. *Exp. Eye Res.* **46**, 431–42.

Zimmermann, D. R., Trueb, B., Winterhalter, K. H., Witmer, R. and Fischer, R. W. (1986). Type VI collagen is a major component of the human cornea. *FEBS Lett.* **197**, 55–8.